Chemical Engineering Science 117 (2014) 114–124

Contents lists available at ScienceDirect

Chemical Engineering Science

journal homepage: www.elsevier.com/locate/ces

The influence of Marangoni convection on fluid dynamics of oscillating single rising droplets

Roland F. Engberg [a], Mirco Wegener [b], Eugeny Y. Kenig [a,c,*]

[a] Chair of Fluid Process Engineering, University of Paderborn, Pohlweg 55, 33098 Paderborn, Germany
[b] Chair of Chemical & Process Engineering, Technische Universität Berlin, Ackerstraße 71-76, 13355 Berlin, Germany
[c] Gubkin Russian State University of Oil and Gas, Moscow, Russian Federation

HIGHLIGHTS

- 3D simulations illuminating the impact of solutal Marangoni effects on oscillating droplets.
- Validation of numerical results with experiments in the toluene/acetone/water system.
- The initial droplet shape influences the rise behaviour of oscillating droplets.
- Irregular flow patterns induced by Maragoni convection trigger rise path oscillations.
- Excellent prediction of characteristic velocity for different solute concentrations.

GRAPHICAL ABSTRACT

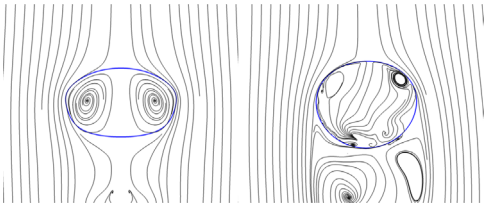

ARTICLE INFO

Article history:
Received 24 February 2014
Received in revised form
23 April 2014
Accepted 27 May 2014
Available online 4 June 2014

Keywords:
Droplet
Marangoni convection
Mass transfer
CFD
Level set
Extraction

ABSTRACT

The impact of solutal Marangoni convection on fluid dynamics and mass transfer cannot be described by means of analytical methods, due to their inherently three-dimensional, highly unsteady and non-linear nature. Hence, experimental and – to an increasing degree – numerical efforts are needed to reveal the underlying phenomena. This paper presents three-dimensional numerical simulations of an oscillating single droplet rising in a quiescent ambient liquid, with and without the Marangoni effect induced by the interfacial mass transfer of a solute. For the simulations, a CFD code based on the level set method was implemented in the open-source software OpenFOAM®. Experiments in the oscillating droplet regime have been carried out with the toluene/acetone/water system for different initial solute concentrations (reflecting different strengths of Marangoni convection) to obtain data for the validation of the numerical results. Comparisons between experimental and simulation results regarding the velocity, shape and trajectories of a rising droplet show a good qualitative and quantitative agreement. This will provide a basis for comprehensive mass transfer studies at deformable and oscillating droplets with simultaneous interfacial phenomena, such as Marangoni convection and surfactant adsorption, in the future.

1. Introduction

In liquid–liquid extraction processes, one phase is usually dispersed as droplets rising or sedimenting in a continuous phase. Therefore, the design of liquid–liquid extraction processes is often based on mass transfer and fluid dynamic properties of droplet

* Corresponding author at: Chair of Fluid Process Engineering, University of Paderborn, Pohlweg 55, 33098 Paderborn, Germany.
E-mail addresses: rolandengberg@gmx.de (R.F. Engberg), mirco.wegener@alumni.tu-berlin.de (M. Wegener), eugeny.kenig@uni-paderborn.de (E.Y. Kenig).

http://dx.doi.org/10.1016/j.ces.2014.05.047
0009-2509/

swarms. These properties are usually derived from correlations developed for single droplets. Consequently, a detailed knowledge of the underlying transport phenomena is essential for a physically meaningful derivation of correlations. In this respect, a combined numerical and experimental analysis seems to be a very promising approach. While numerical simulations provide an in-depth insight into transport phenomena and local data, thorough experiments are indispensable for model validation. Furthermore, experimental studies remain the primary basis for the description of the overall extraction process.

Recent combined numerical and experimental investigations of droplet fluid dynamics were carried out by Bertakis et al. (2010) for the *n*-butanol/water system, by Bäumler et al. (2011) for the *n*-butyl acetate/water system and by Eiswirth et al. (2011, 2013) for the toluene/water system.

In some cases, the fluid dynamic behaviour of droplets is not influenced by interfacial mass transfer. However, this situation changes when mass transfer leads to gradients of the interfacial tension, evoking Marangoni convection. Previous works (Wegener et al., 2007, 2009b,c) in the spherical droplet regime using the toluene/acetone/water system have shown that Marangoni convection influences the fluid dynamic behaviour in a characteristic manner. Interfacial tension gradients induce additional shear stresses at the interface which disturb the development of internal circulations in the droplet and increase the drag coefficient. Thus, the droplet rises slower than a solute-free droplet. For non-oscillating droplets it was observed that the higher the initial solute concentration was, the stronger was the Marangoni effect and the larger were deviations from the corresponding terminal rise velocity of a solute-free droplet. In the extreme case, above a certain critical initial solute concentration, the droplets accelerated only to a velocity level which corresponded to the terminal velocity of a comparable rigid sphere.

Due to the strong coupling of momentum and mass transfer, Marangoni effects are highly non-linear and unsteady. Generally, Marangoni convection is strongest in the beginning, when the drop is formed at and detached from a capillary, and large concentration gradients appear. With progressing mass transfer, Marangoni effects decrease. Once the Marangoni convection diminished, a reacceleration occurred which can be explained with the onset of a toroidal internal circulation and, consequently, the decrease of the drag coefficient. The time of reacceleration was clearly measurable and was determined to be a linear function of the ratio of droplet diameter to initial solute concentration (Wegener et al., 2009b).

Previous experimental studies of Marangoni convection at single droplets in liquid–liquid systems comprise investigations of mass transfer for circulating and oscillating droplets, e.g. by Steiner et al. (1990), Henschke and Pfennig (1999), Wegener et al. (2007) and Wegener and Paschedag (2011). Moreover, Wegener et al. (2009a) investigated the mass transfer enhancement due to Marangoni convection during droplet formation. Wegener et al. (2007) and Wegener et al. (2009b) presented an experimental study on the fluid dynamic behaviour of circulating droplets.

Burghoff and Kenig (2006) performed CFD simulations of droplets taking Marangoni and cross-effects of multicomponent diffusion into account. The simulations were two-dimensional and a spherical droplet shape was assumed.

Wang et al. (2011) presented experimental and numerical results for Marangoni convection at single droplets. Using a level set based CFD code, they were able to take droplet deformation into account. The investigation was limited to small circulating droplets and two-dimensional simulations. Furthermore, Wang et al. (2013) used the same CFD code to simulate mass transfer and Marangoni effects during droplet formation in a two-dimensional axially symmetrical domain. The results were in good agreement with their own experimental data.

Wegener et al. (2009c) pointed out that Marangoni convection is a three-dimensional phenomenon and, consequently, simulated spherical droplets in a full three-dimensional domain. Regarding mass transfer and rise velocity, a good agreement with the experimental data of Wegener et al. (2007) was achieved. Deviations from a straight rise path were not taken into account.

In two recent studies, Engberg et al. (2014a,b) presented full three-dimensional CFD simulations of deformable droplets. The studies were limited to circulating droplets with small deformations. While the rise velocity was in very good agreement with the experimental data of Wegener et al. (2007), the results for mass transfer were less satisfactory. For the first time, a lateral break-out in the droplet path, indicating the decrease of Marangoni convection and observed in previous experimental studies by Wegener et al. (2007, 2009b), was reproduced by simulations.

In comparison with spherical droplets (or droplets with only slight deformations), the fluid dynamic behaviour of oscillating droplets is substantially different and less predictable, because the droplet shape is unsteady, imposing different flow patterns by itself. It should be noted that, to the best of our knowledge, the impact of Marangoni convection on the fluid dynamic behaviour of oscillating droplets has not been studied yet and that the literature regarding oscillating droplets is scarce.

In this work, the influence of Marangoni convection on the fluid dynamic behaviour was examined experimentally and numerically. Toluene droplets with a diameter of 5 mm rising in water were investigated. Marangoni convection was induced by the transferred component acetone, and the influence of the initial solute concentration was studied. In the experiments, the droplets were filmed with high-speed cameras, providing detailed insights into the fluid dynamic behaviour. For the simulations, a CFD code based on the level set method was developed and implemented in the open-source CFD-package OpenFOAM®. Droplets were simulated fully three-dimensional, and the results regarding droplet rise velocity, droplet shapes and trajectories were compared with the experimental data.

2. Mathematical model and numerical method

2.1. Moving interface

The level set method (Osher and Sethian, 1988) employs a scalar function $\psi(\mathbf{x},t)$ to indicate whether a point $\mathbf{x}$ is located in the dispersed phase Ω_d or the continuous phase Ω_c at time t:

$$\psi(\mathbf{x},t)<0 \quad \text{in the dispersed phase } (\mathbf{x}\in\Omega_d) \tag{1}$$

$$\psi(\mathbf{x},t)>0 \quad \text{in the continuous phase } (\mathbf{x}\in\Omega_c) \tag{2}$$

Consequently, the interface $\partial\Omega=\partial\Omega_c\cap\partial\Omega_d$ is defined by the isocontour $\psi(\mathbf{x},t)=0$.

The movement of the interface can be described with a simple advection equation:

$$\frac{\partial\psi}{\partial t}+\mathbf{v}\cdot\nabla\psi=0 \tag{3}$$

where $\mathbf{v}$ denotes the velocity field.

If physical properties are to be expressed through the level set function, a signed distance function is a particularly useful choice for ψ. As a signed distance function, ψ has the following properties:

$$|\psi(\mathbf{x})|=\min(|\mathbf{x}-\mathbf{x}_I|) \text{ for all } \mathbf{x}_I\in\partial\Omega \tag{4}$$

$$|\nabla\psi|=1 \tag{5}$$

These properties are usually lost during the advection of ψ and have to be restored. For this purpose, the following partial

differential equation was solved numerically after the transport of ψ with Eq. (3):

$$\frac{\partial \psi}{\partial \tau} = \frac{\psi_0}{\sqrt{\psi_0^2 + \Delta x^2}}(1 - |\nabla \psi|) + \tilde{\mathcal{F}} \tag{6}$$

where τ is pseudo-time, Δx is grid spacing, $\tilde{\mathcal{F}}$ is a forcing term and ψ_0 is the initial condition

$$\psi_0 = \psi(\mathbf{x}, \tau = 0) \tag{7}$$

This procedure called reinitialisation was introduced by Sussman et al. (1994). Eq. (6) was discretised in pseudo-time with a simple explicit Euler scheme with a step size of $\Delta\tau = \Delta x/2$. For the spatial derivatives, the third-order WENO scheme of Jiang and Peng (2000) was used.

A well-known drawback of the level set method is the artificial volume change of the phases stemming from numerical inaccuracies when the advection and reinitialisation equations (Eqs. (3), (6)) are solved. To overcome this drawback, two methods were used simultaneously in this work. The original reinitialisation equation of Sussman et al. (1994) was augmented with an additional term $\tilde{\mathcal{F}}$. This forcing term was recently suggested by Hartmann et al. (2010). It helps to reduce the volume change during reinitialisation. As recommended by Hartmann et al. (2010), the forcing term was evaluated according to the high-order constrained reinitialisation scheme 2 (HCR-2) in a predictor–corrector procedure.

Additionally, an interface shift, as proposed by Gross (2008), was implemented. After the reinitialisation, a new level set function ψ_{new} was calculated by subtracting a correction $\tilde{\psi}$ from the reinitialised level set function ψ:

$$\psi_{new} = \psi(\mathbf{x}, t) - \tilde{\psi} \tag{8}$$

To ensure that the volume described by ψ_{new} was equal to the initial droplet volume with a relative tolerance of 10^{-7}, the correction $\tilde{\psi}$ was determined iteratively with a regula falsi algorithm. The shifted level set function ψ_{new} was then used for the subsequent calculations.

2.2. Fluid dynamics

The liquid phases considered in this study consist of toluene, water and acetone and are Newtonian. Consequently, the incompressible flow can be described with the mass continuity (9) and the Navier–Stokes (10) equations:

$$\nabla \cdot \mathbf{v} = 0 \tag{9}$$

$$\frac{\partial(\rho \mathbf{v})}{\partial t} + \rho \mathbf{a} + (\rho \mathbf{v} \cdot \nabla)\mathbf{v} = \nabla \cdot (\eta(\nabla \mathbf{v} + \nabla \mathbf{v}^T)) - \nabla p - \rho \mathbf{g} + \mathbf{F}_\sigma \tag{10}$$

where ρ denotes density, η viscosity, p pressure, $\mathbf{g}$ gravitational acceleration and $\mathbf{F}_\sigma$ the forces induced by the interfacial tension σ. A modified pressure without hydrostatic contribution $p^* = p - \rho \mathbf{g} \cdot \mathbf{x}$ is used in the simulations to simplify the specification of boundary conditions (cf. Rusche, 2002). For an efficient simulation of long rise times, the computational domain follows the droplet during its rise. This moving reference frame leads to an acceleration term $\mathbf{a}$ in the momentum equation (10). A detailed description of its calculation can be found in Engberg et al. (2014b).

A smoothed Heaviside function H_ϵ was employed to calculate density and viscosity in the two-phase domain:

$$H_\epsilon(\psi) = \begin{cases} 0 & \text{if } \psi < -\epsilon \\ \frac{1}{2} + \frac{\psi}{2\epsilon} + \frac{1}{2\pi} \sin\left(\frac{\pi\psi}{\epsilon}\right) & \text{if } |\psi| \le \epsilon \\ 1 & \text{if } \psi > \epsilon \end{cases} \tag{11}$$

The smoothing parameter ϵ was set to $\epsilon = 1.5\Delta x$ for the simulations.

Density ρ was calculated with

$$\rho = \rho_d + (\rho_c - \rho_d) H_\epsilon(\psi) \tag{12}$$

Following the method suggested by Kothe (1998), viscosity was calculated from its harmonic and arithmetic averages according to the relative orientation of the interface and the cell face (Engberg et al., 2014b).

Regarding the interfacial forces, we chose the approach of Hayashi and Tomiyama (2012) and implemented different methods for the normal and the tangential components. The ghost fluid method (GFM) of Kang et al. (2000) was used for the forces acting normal to the interface. Consequently, when the interface was located between two cell centres i and $i+1$, the discrete pressure gradient at the cell face $i+1/2$ was given by

$$\left(\frac{\partial p}{\partial x}\right)_{i+1/2} \approx \frac{p_{i+1} - p_i}{\Delta x} - \frac{\sigma \kappa_{I,i+1/2}}{\Delta x} \tag{13}$$

The last term on the right-hand side of Eq. (13) accounts for the interfacial forces acting normally to the interface. The interfacial forces are proportional to the interfacial tension and the curvature κ, which is defined as the divergence of the interface unit normal $\mathbf{n}$ calculated from the level set function:

$$\mathbf{n} = \frac{\nabla \psi}{|\nabla \psi|} \tag{14}$$

$$\kappa = -\nabla \cdot \mathbf{n} \tag{15}$$

For the cell centred curvatures $\overline{\kappa}_i$, the curvature was integrated over each finite volume V_i to obtain an averaged value. Using the Gaussian theorem yields:

$$\overline{\kappa}_i = -\frac{1}{V_i}\int_{V_i} \nabla \cdot \mathbf{n}\, dV \tag{16}$$

$$= -\frac{1}{V_i}\int_S \mathbf{n} \cdot d\mathbf{S} \tag{17}$$

The curvature at the interface $\kappa_{I,i+1/2}$ was interpolated from the cell centred values (cf. Liu et al., 2000; Francois et al., 2006):

$$\kappa_{I,i+1/2} = \frac{\overline{\kappa}_i |\psi_{i+1}| + \overline{\kappa}_{i+1} |\psi_i|}{|\psi_i| + |\psi_{i+1}|} \tag{18}$$

The implementation of the normal interfacial forces in Eq. (10) can lead to pressure oscillations at the interface and evoke unphysical spurious currents (Brackbill et al., 1992; Francois et al., 2006) which act similar to Marangoni convection. Consequently, it has to be ensured that these currents are limited and do not interfere with Marangoni effects. The strength of spurious currents depends on the implementation of the interfacial forces and the curvature approximation (Francois et al., 2006). In a previous work, our code was validated with the static droplet test case and droplet rise velocities (Engberg and Kenig, 2014). Due to the GFM and the good curvature approximation with the level set method, the influence of spurious currents was found to be small and an excellent agreement with recent numerical and experimental results for rise velocities in three different liquid–liquid systems was achieved.

For the forces acting tangentially to the interface $\mathbf{F}_{\sigma,t}$, the continuum surface force (CSF) model of Brackbill et al. (1992) was chosen:

$$\mathbf{F}_{\sigma,t} = (\nabla \sigma - \mathbf{n}(\mathbf{n} \cdot \nabla \sigma))\delta_\epsilon(\psi) \tag{19}$$

where the smoothed delta function δ_ϵ was given by

$$\delta_\epsilon(\psi) = \begin{cases} 0 & \text{if } |\psi| > \epsilon \\ \frac{1}{2\epsilon} + \frac{1}{2\epsilon} \cos\left(\frac{\pi\psi}{\epsilon}\right) & \text{if } |\psi| \le \epsilon \end{cases} \tag{20}$$

Due to the smoothed delta function, the interfacial forces are transformed in volume forces acting in a small region at the

interface. The tangential forces (19) may evoke Marangoni convection if the interfacial tension varies.

The Pressure Implicit with Splitting of Operators (PISO)-algorithm of Issa (1986) was used for pressure–velocity coupling. In all simulations, three corrector steps were performed with the PISO-loop.

2.3. Mass transport

In this study, low concentrations of acetone were considered. Hence, both phases can be treated as diluted systems, which simplifies the mathematical description of mass transfer phenomena.

The interfacial boundary conditions for mass transfer are the thermodynamic equilibrium (21), which results in a concentration jump at the interface proportional to the distribution coefficient K, and the continuity of diffusional fluxes (22):

$$c_{Ad} = K c_{Ac} \tag{21}$$

$$D_{Ad} \nabla c_{Ad} \cdot \mathbf{n} = D_{Ac} \nabla c_{Ac} \cdot \mathbf{n} \tag{22}$$

In contrast to front tracking methods, front capturing methods like the level set approach do not provide computational nodes located at the interface where boundary conditions could be implemented directly. Therefore, fulfilling the boundary condition (Eqs. (21), (22)) is particularly challenging in a front capturing framework. Haroun (2008) derived a single-field formulation for mass transfer (cf. Haroun et al. 2010a,b) which was used in the present work. The mass transport in the entire computational domain is described in terms of the mixture concentration $C = H_\epsilon c_{Ac} + (1 - H_\epsilon) c_{Ad}$:

$$\frac{\partial C}{\partial t} + \nabla \cdot (\mathbf{v} C) = \nabla \cdot (D_m \nabla C) - \nabla \cdot \left(D_m \frac{1-K}{H_\epsilon + K(1-H_\epsilon)} C \nabla H_\epsilon \right) \tag{23}$$

The last term on the right-hand side accounts for the interfacial boundary conditions (Eqs. (21), (22)). It should be noted that the original formulation of Haroun (2008) is based on the volume-of-fluid method and employs the volume fraction of one phase. As the volume fraction was not available in the level set method, it was approximated with the Heaviside function H_ϵ. Similar to the viscosity, the diffusivity D_m was interpolated with the method of Kothe (1998).

Table 1
Physical properties at a temperature of 25 °C given by Misek et al. (1985).

Phase	Density (kg/m^3)	Dynamic viscosity (10^{-4} Pa s)	Diffusivity of acetone (10^{-9} m^2/s)
Toluene phase	862.30	5.520	2.90
Aqueous phase	997.02	8.903	1.25

2.4. Simulation

The governing equations were implemented in the open-source CFD-toolbox OpenFOAM® and solved in a sequential manner. Full three-dimensional simulations of toluene droplets with an initial diameter of $d_0 = 5$ mm rising in water were carried out. The transport direction was $d \rightarrow c$, and various initial concentrations of acetone were simulated. Except for the interfacial tension, the physical properties were assumed to be independent of the acetone concentration and, consequently, the properties of pure substances were employed. This is in line with the assumption of a dilute system. The physical properties taken from Misek et al. (1985) are compiled in Table 1. For the interfacial tension, an exponential function of the acetone concentration in toluene c_{AT} was fitted to the data of Misek et al. (1985):

$$\sigma = 0.0025 + 0.03285 \exp(-0.0145 c_{AT}) \tag{24}$$

where the units of c_{AT} and σ are g/L and N/m, respectively. In accordance with previous studies (Wegener et al., 2009c; Engberg et al., 2014a), a distribution coefficient $K = 0.63$ was used.

The computational domain was $12 d_0$ high and $8 d_0$ deep and wide. The grid consisted of cuboid cells and was refined in the vicinity of the interface, cf. Fig. 1. Due to the moving reference frame (cf. Section 2.2), the interface remained in the refined region. For the simulations without Marangoni convection, a grid

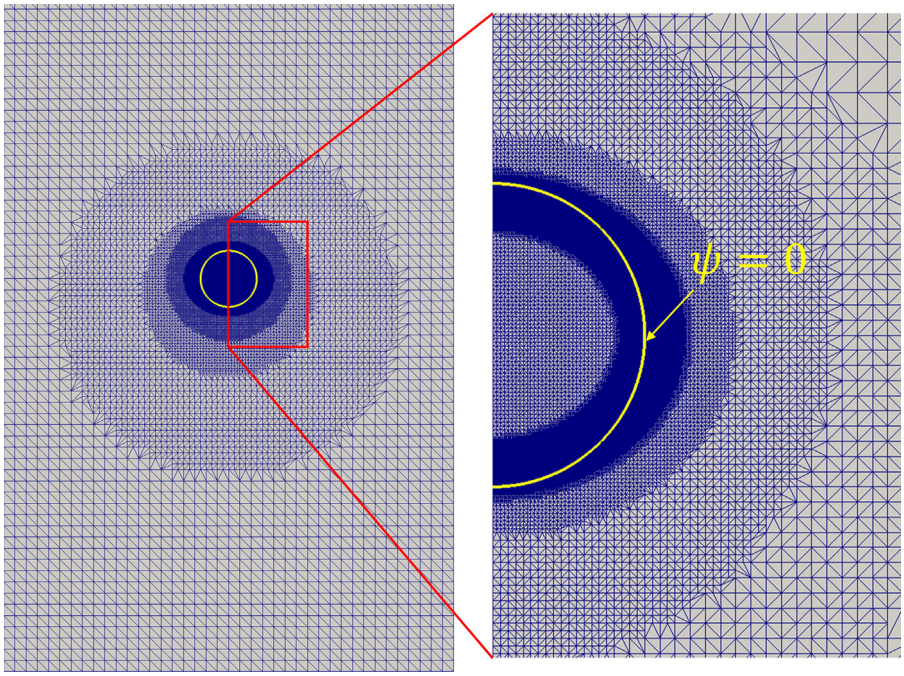

Fig. 1. A slice through the three-dimensional computational domain. The grid consists of cuboid cells (due to the post processing program, the cells appear as triangles) and is refined in the vicinity of the interface to a grid spacing of approximately 16 μm.

spacing of $\Delta x = d_0/80 = 62.5$ μm was chosen which was found to be reasonable for this purpose (Engberg and Kenig, 2014). In a previous study (Engberg et al., 2014b), we showed that a grid spacing of approximately 16 μm is sufficient to capture the characteristic fluid dynamic behaviour of a droplet dominated by Marangoni convection. Consequently, this grid spacing was used for simulations with Marangoni convection in this study, leading to more than 22 million cells. Owing to this large mesh, a further grid refinement to approximately 2 μm, which would be required to resolve mass transfer properly (Engberg et al., 2014b), is currently not feasible. A remedy would be an adaptive mesh refinement, which is, however, not implemented in the current code, but will be adopted for future work.

For the simulations with Marangoni convection, the droplet was initialised as a sphere (cf. Fig. 2(a)). In addition, an alternative initialisation as an ellipsoid (ratio of principal axes: 0.7) rotated by 70° around the y-axis was used for simulations without Marangoni convection to investigate the influence of the initial droplet shape on its fluid dynamic behaviour (cf. Fig. 2(b)). The distance from the centre of the droplet to the bottom of the computational domain was $7d_0$. The initial concentration field was constant (c_{A0}) within the droplet and zero in the rest of the domain.

A schematic representation of the boundary conditions is shown in Fig. 2(c). The velocity at the top and the sides of the computational domain was equal to the frame velocity $\mathbf{v}_F$. At the bottom of the domain, a zero gradient condition was employed for velocity. Zero gradient conditions were also appropriate for the level set function and the concentration at the top, bottom and sides. The boundary conditions for the modified pressure were a constant reference pressure at the bottom and zero gradient at the top and sides.

Eqs. (3), (9), (10) and (23) were discretised with the finite volume method. For convective terms, the Gamma scheme introduced by Jasak et al. (1999) was used. An implicit Euler scheme with a constant time step of 50 ms for the coarse grid (62.5 μm) and 15 ms for the fine grid (16 μm) was employed to discretise time, leading to a maximum Courant number of 0.3.

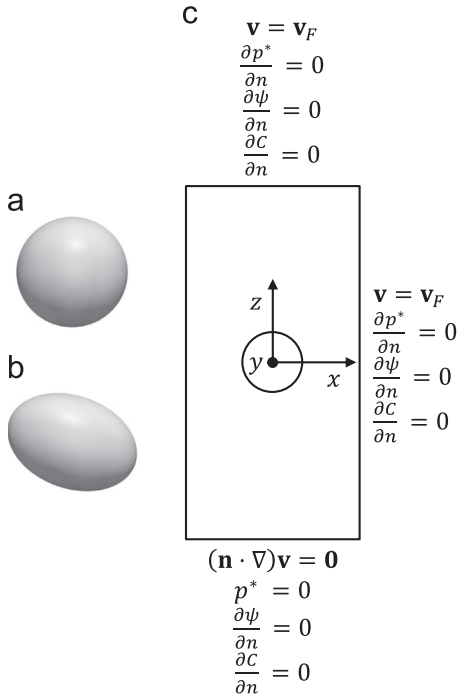

Fig. 2. The droplet was initialised either as (a) a sphere or (b) a rotated ellipsoid. (c) Schematic representation of the computational domain with the boundary conditions for the simulations.

3. Experimental setup

The experimental setup is displayed in Fig. 3. The left-hand side shows the front view, while the right-hand side depicts the top view focusing on the arrangement of the high-speed cameras and the background lighting. All measurements were carried out in a glass column (1) (1000 mm height, 75 mm in diameter). The column diameter was large enough to ensure a negligible influence of the column wall on the drop rise velocity (Wegener et al., 2010). The preponderant part of the column was surrounded by a cooling jacket (2) in which anhydrous glycerol was circulated to maintain a constant temperature and to match the refractive index of the borosilicate glass of the column in order to minimise the distortion effect of the curved column wall. Behind the column, background lighting (3) was provided. It consisted of two boxes (one for each camera plane), each containing two long fluorescent lamps with low thermal radiation and in optimal distance to one another. A constant image brightness and quality was obtained by using a power supply unit at an operation frequency of 40 kHz. Two Photonfocus MV-752-160 high-speed cameras (4, 5) were used, both operating at a frame rate of 100 Hz in master–slave configuration. The master captured the droplet path in the x-z-plane, while the slave recorded the path in the y-z-plane. The distance between the camera and column was chosen in a manner that the entire droplet path through the column including the formation at the capillary could be captured.

For all experiments, the rise of water-saturated toluene droplets (equivalent diameter: 5 mm) in toluene-saturated water was investigated. The solute was acetone with different initial concentrations varying from 0 to 60 g/L in the organic phase. The mass transfer direction was from the dispersed into the aqueous phase. Contaminations in technical grade chemicals were found to be sufficient to have a significant impact on mass transfer and the fluid dynamic behaviour of the droplets, because they preferably adsorbed at the droplet interface. Therefore, high purity chemicals had to be used: toluene p.a. ≥ 99.9%, acetone p.a. ≥ 99.8%, both provided by Merck, and deionised water with a specific resistance of 18.3 MΩ cm. It was also found to be beneficial that the parts of the experimental setup in contact with the chemicals were made

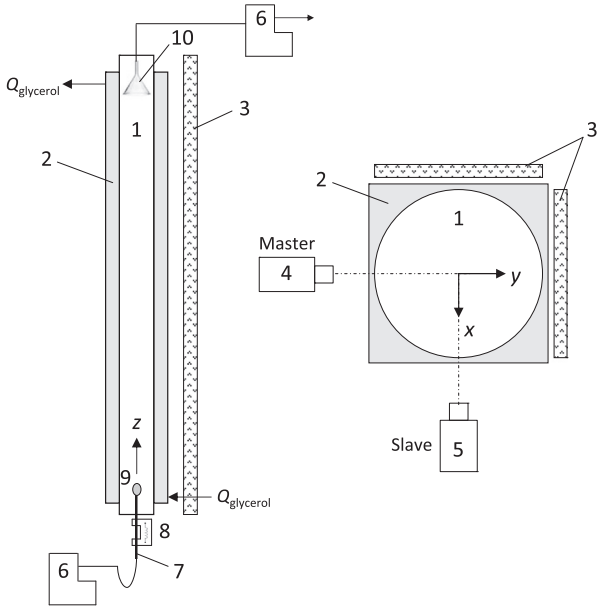

Fig. 3. Schematic of the droplet column used in the experiments. Left: front view, right: top view. 1: glass column, 2: cooling jacket with glycerol flow rate $Q_{glycerol}$, 3: background light, 4: high-speed camera, master, 5: high-speed camera, slave, 6: precision dosing pumps, 7: capillary, 8: solenoid, 9: droplet, and 10: glass funnel.

from inert materials, such as Teflon or glass. The capillary material was stainless steel. A thorough cleaning procedure was developed including the containers in which the chemicals were kept, even if it was only for a short time, e.g. for mutual saturation. The success of the cleaning procedure was checked by measuring the drop rise velocity of acetone-free toluene droplets, whose terminal velocity as a function of droplet diameter was measured and confirmed by simulations in two earlier studies (Bäumler et al., 2011; Wegener et al., 2010).

The toluene droplets (9) were produced in the following manner. The toluene phase was kept initially in a phial. A precision dosing pump (6) (Hamilton PSD/2 module using gas tight syringes with Teflon tip) pumped the required volume through a Teflon hose which was connected to the stainless steel capillary (7) (inner diameter 2 mm, outer diameter 3 mm). The droplet detachment was achieved by using a solenoid device (8) which retracted quickly the flexibly mounted capillary. In this manner, droplets of equal size per detachment were obtained. Due to the detachment process, an initial droplet deformation occurred. The droplet rose within the column and was caught by a funnel (10) from which the dispersed phase was withdrawn, droplet by droplet, using a second precision dosing pump (6). The whole droplet formation, detachment and withdrawal process was fully automated. At least 20 sequences were recorded in each case.

The trajectory of the droplet through the column was recorded simultaneously by both cameras. Prior to each next droplet formation, the stored sequence of images had to be transferred to the hard disc of a computer to empty the internal memory of the cameras. The images were analysed using an image processing tool (Image-Pro Plus). Thereto, a reference frame was subtracted from each original image of the sequence to facilitate the transformation into a binary image. After image processing, the x,z- and the y,z-position of the mass centre of the droplet were available as functions of time.

4. Results

4.1. Rise velocity

As shown in previous studies (Bäumler et al., 2011; Wegener et al., 2010), toluene droplets with $d_0 \geq 4.4$ mm rising in water show shape and velocity oscillations. A droplet diameter of $d_0 = 4.4$ mm leads to a Weber number of 3.8, which is in good agreement with the critical value of 4.08 for the onset of oscillations given by Winnikow and Chao (1966).

The transient rise velocity of a toluene droplet with $d_0 = 5$ mm without Marangoni convection is shown in Fig. 4. In the experiments, the droplet accelerates quickly to a maximum velocity of approximately 173 mm/s. After a short deceleration, the droplet reaches its characteristic (or mean) rise velocity of 162 mm/s, which can be calculated as

$$v_{char} = \frac{\Delta z}{\Delta t} \tag{25}$$

where Δz is the change in the droplet rise height within a period Δt. The frequency of the velocity oscillations is approximately 1 Hz and the amplitude is 5 mm/s.

The simulated rise velocity of a droplet initialised as a sphere is shown in Fig. 4(a). While the simulated characteristic rise velocity is relatively close to the experimental value, maximum velocity, frequency and amplitude are significantly higher. Even though numerical investigations of oscillating droplets are relatively scarce in the literature, similar high-frequency oscillations were also found in other works, e.g. Bäumler et al. (2011), Dijkhuizen et al. (2005), and Engberg and Kenig (2014). We are yet to understand whether these oscillations occur in reality or stem from numerical problems. Due to the high frequencies, an experimental proof is currently not feasible, even when high-speed cameras are used. What does become apparent in the present study, however, is that the strength of the high-frequency oscillations is influenced by the initial droplet shape. This can be deduced from Fig. 4(b) where the simulated rise velocity of a droplet initialised as a rotated ellipsoid is shown together with experimental data. The high-frequency oscillations remain, but the amplitude is clearly lower. While the simulated maximum rise velocity is slightly lower than the experimental result, the characteristic rise velocities are in good agreement.

An analysis of droplet cross-sections reveals that the two droplet initialisations result in different shape oscillations. As shown in Fig. 5 (upper row), the droplet initialised as a sphere largely remains rotationally symmetric in the x–y-plane and oscillations are dominated by movements in the z-direction (i.e. the direction of gravitational acceleration). In contrast, the droplet initialised as a rotated ellipsoid shows distinct asymmetries in the x–y-plane, cf. Fig. 5 (lower row). These shape oscillations seem to lead to lower velocity amplitudes.

After a rise time of 4 s, the high-frequency oscillations vanish almost completely, and a secondary velocity oscillation with lower amplitude and frequency develops. This coincides with the onset of a droplet rotation around its centre axis, as can be deduced from

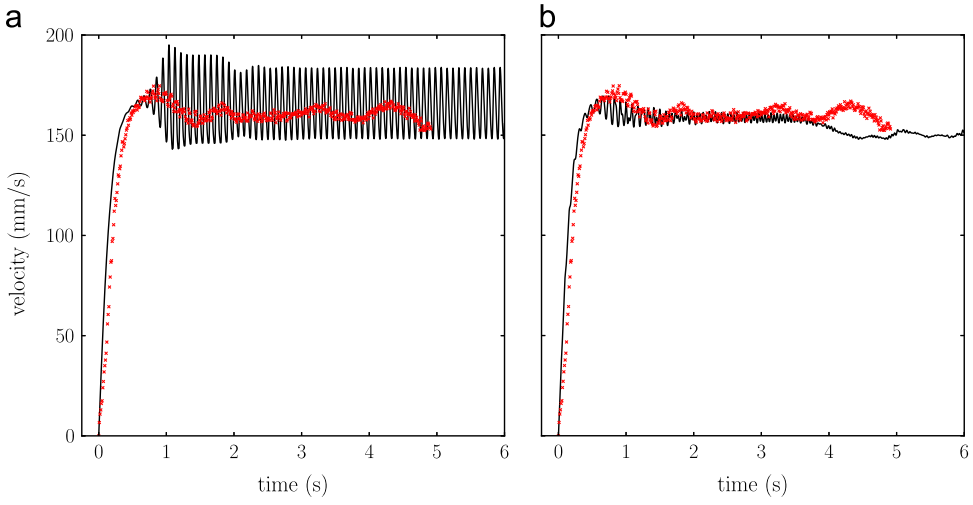

Fig. 4. Transient rise velocity of a toluene droplet with $d_0 = 5$ mm in water: Experimental (×) and simulation (−) results; the simulated droplet was initialised (a) as a sphere and (b) as a rotated ellipsoid.

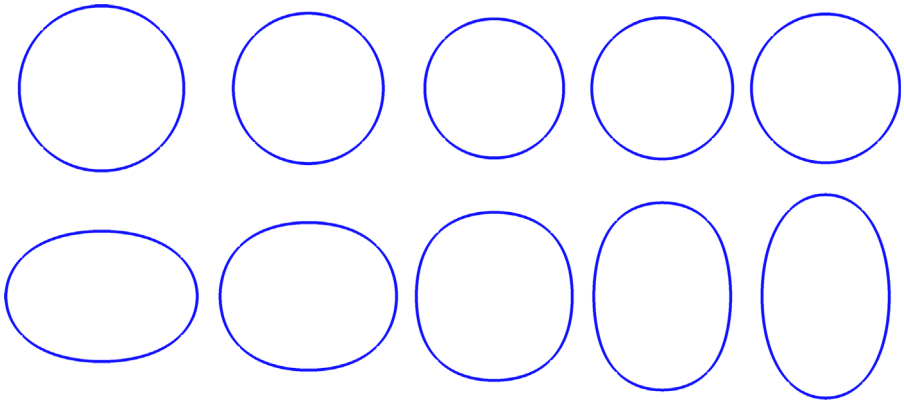

Fig. 5. Simulated droplet cross-sections in the x–y-plane at times 1.0 s, 1.1 s, 1.2 s, 1.3 s and 1.4 s for a droplet initialised as a sphere (upper row) and as a rotated ellipsoid (lower row).

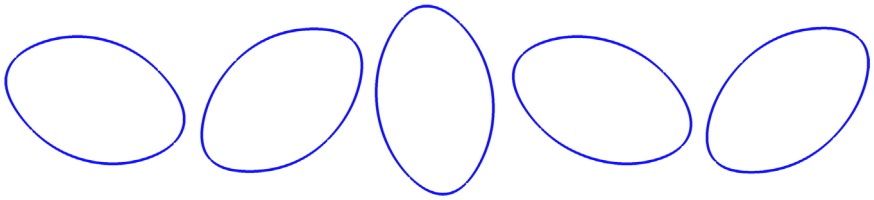

Fig. 6. Simulated droplet cross-sections in the x–y-plane at times 4.0 s, 4.1 s, 4.2 s, 4.3 s and 4.4 s (from left to right) for a droplet initialised as a rotated ellipsoid.

the droplet cross-sections shown in Fig. 6. Interestingly, the frequency of rotation is approximately 1 Hz, which is in accordance with the experimental data for the frequency of velocity oscillations. Krishna et al. (1959) observed rotations of oscillating droplets in various liquid/liquid systems. Similar rotations can also be found in the experimental droplet shapes in our work, as shown in Section 4.2.

It is likely that the extreme velocity oscillations found for a droplet initialised as a sphere can only develop under the ideal symmetric conditions applied in a numerical simulation, whereas in experiments, small disturbances and deformations during the droplet formation may easily lead to asymmetries.

The simulation results indicate that the rise behaviour of a droplet apparently depends on the initial droplet shape. Tomiyama et al. (2002) and Wu and Gharib (2002) found a significant impact of the initial shape of a bubble on its rise behaviour in water. Moreover, for single droplets in liquid/liquid systems, Wegener et al. (2010) found evidence that the droplet fluid dynamics is influenced by the initial droplet deformation. Therefore, the influence of the initial droplet shape on its rise behaviour will be studied in a future investigation.

The impact of the initial acetone concentration on the transient rise velocity is shown in Fig. 7. While the maximum velocities of droplets with lower initial concentrations occasionally reach values similar to the case with constant interfacial tension, Marangoni convection clearly reduces the characteristic rise velocity. This effect becomes more pronounced for higher initial concentrations. Fig. 8 illustrates the reduction of the characteristic rise velocity due to Marangoni convection. Furthermore, it shows that, for the high initial concentrations of 30 g/L and 60 g/L, the characteristic velocities do not change in a significant manner anymore. Higher initial concentrations also lead to more regular oscillations with smaller amplitudes and higher frequencies, as can be deduced from Fig. 7.

Simulation results for the transient rise velocity with three different initial concentrations are shown in Fig. 9. In accordance with the experimental results, Marangoni convection reduces the rise velocity. Compared with the experimental data, however, the

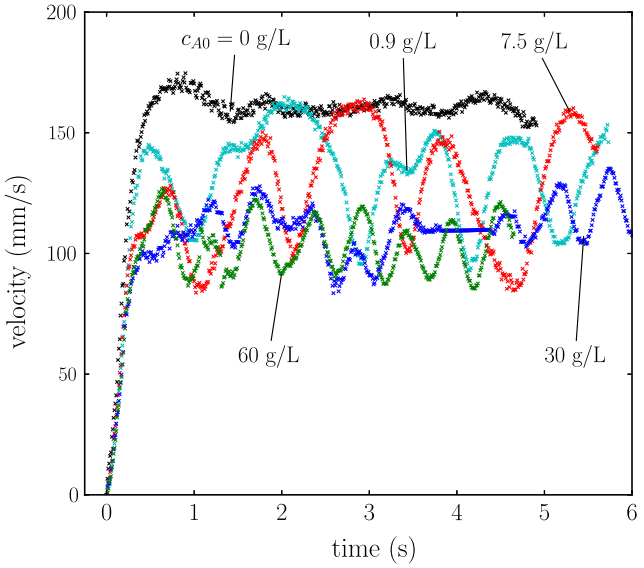

Fig. 7. Experimental results for the transient rise velocity of toluene droplets in water with $d_0 = 5$ mm and various initial concentrations of acetone. The rise velocity of a droplet with constant interfacial tension ($c_{A0} = 0$ g/L) is shown for comparison.

simulated rise velocities show only mild oscillations with lower amplitudes and higher frequencies. Nevertheless, it can be stated that the general trend is represented by the simulations, and the simulated characteristic rise velocities agree well with the corresponding experimental data, as can be seen in Fig. 8. It should be kept in mind that Marangoni convection leads to a strong coupling of momentum and mass transfer. As noted in Section 2.4, the grid is too coarse to resolve mass transfer properly and, consequently, the simulated mass transfer rates are significantly higher than in the experiments. It is likely that a finer grid would lead to a better quantitative agreement of the transient rise velocities.

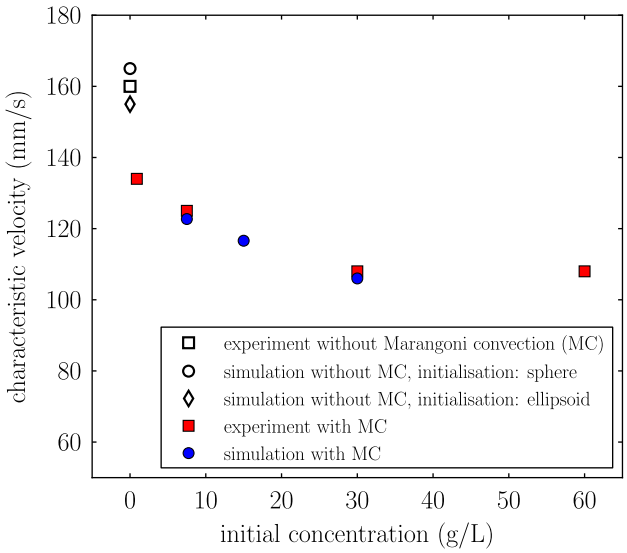

Fig. 8. The characteristic rise velocity of toluene droplets ($d_0 = 5$ mm) in water as a function of the initial acetone concentration. The experimental data are averages of 15 sequences. Filled and unfilled symbols denote cases with and without Marangoni convection, respectively.

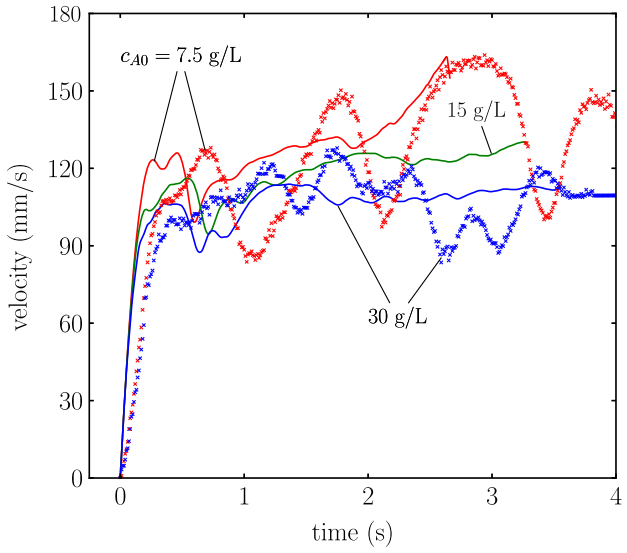

Fig. 9. Simulated transient rise velocity of toluene droplets in water with $d_0 = 5$ mm and three different initial concentrations of acetone (lines). The experimental results for $c_{A0} = 7.5$ g/L and $c_{A0} = 30$ g/L are shown for comparison (symbols).

Due to the higher mass transfer rates, the rise time dominated by Marangoni convection is shorter than in the experiments. When Marangoni effects decrease, the droplet accelerates and deforms stronger. Thus, the interface leaves the finest region of the mesh, and the simulation breaks down. This can be seen in the transient rise velocity for $c_{A0} = 7.5$ g/L at $t \approx 2.6$ s in Fig. 9.

The reduced rise velocity due to Marangoni convection was also found for smaller circulating droplets in previous studies (Wegener et al., 2007, 2009b,c; Engberg et al., 2014b). Fig. 10 helps to understand this effect. In simulations without Marangoni convection, internal circulations occur, reducing the shear stress acting on the droplet (Fig. 10(a)). In contrast, Marangoni effects lead to irregular flow patterns and disturb the development of internal circulations (Fig. 10(b)). Therefore, the shear stress increases and the rise velocity decreases. As mass transfer proceeds, the variations in interfacial tension diminish and internal circulations develop (Engberg et al., 2014b). While circulating droplets show a distinct second acceleration at this stage, oscillating droplets appear to accelerate gradually when Marangoni effects subside.

4.2. Droplet shapes

Experimental and numerical results for the droplet shapes are displayed in Fig. 11. A toluene droplet ($d_0 = 5$ mm) rising in water, i.e. a case without Marangoni convection, shows strong shape oscillations (Fig. 11(a)). Moreover, deviations from a straight rise path, which are closely connected with an asymmetric deformation of the droplet, can be observed. The simulation of a droplet initialised as a sphere shows shapes similar to the experimental results (Fig. 11(b)), but no asymmetries are apparent. In contrast, the droplet initialised as a rotated ellipsoid deforms asymmetrically (Fig. 11(c)) and rotates around its centre axis. A similar rotation is discernible in the experimental droplet shapes.

As explained in the previous section, Marangoni convection leads to lower characteristic rise velocities. The resulting Weber numbers are lower than the critical value for shape oscillations given by Winnikow and Chao (1966), $We_{crit} = 4.08$. Therefore, experimental and numerical results for cases with Marangoni convection show only mild deformations (cf. Fig. 11(d) and (e)). While the experimental droplet shapes are almost exactly spherical (Fig. 11(d)), the simulated droplets deform stronger and slightly asymmetrically.

4.3. Droplet trajectories

To show the variations observed in the measurements, droplet trajectories of three experimental sequences without Marangoni convection are displayed in terms of the transient x- and y-position in Fig. 12(a) and (b). Considerable deviations from a vertical rise path and path oscillations can be observed, as was already indicated by the corresponding droplet shapes (Fig. 11(a)). Trajectories obtained from simulations without Marangoni convection are displayed in Fig. 12(c) and (d). It should be noted that the scale of the abscissa differs from Fig. 12(a) and (b). For the droplet initialised as a sphere, no deviations from a vertical rise path are discernible. The droplet initialised as a rotated ellipsoid deviates slightly from the vertical in the beginning of its rise, but continues to rise vertically afterwards – despite the fact that asymmetrical deformations are observed (Fig. 11(c)).

Droplet trajectories obtained from experiments and simulations with two different initial concentrations are shown in Fig. 13. In all cases, the droplet rises vertically until an irregular zigzag movement sets in after approximately 0.5 s. Regarding the time and length scale of the path oscillations, a good agreement of experimental and numerical results was achieved. Fig. 14 shows the transition from a vertical rise path to a zigzag trajectory. In the beginning (Fig. 14(a)), the flow patterns are relatively symmetric and a vortex has formed in the wake of the droplet. Marangoni convection leads to increasingly chaotic flow patterns and the droplet deflects laterally (Fig. 14(b) and (c)). The results indicate that, in the case of Marangoni convection, path oscillations are not induced by asymmetrical deformations, but by the irregular flow patterns in the droplet.

5. Conclusions

In this work, the influence of Marangoni convection on the rise behaviour of single oscillating droplets was studied experimentally and numerically. We focussed on toluene droplets with a diameter of 5 mm rising in water. Marangoni convection was induced by concentration differences of the transferred component acetone.

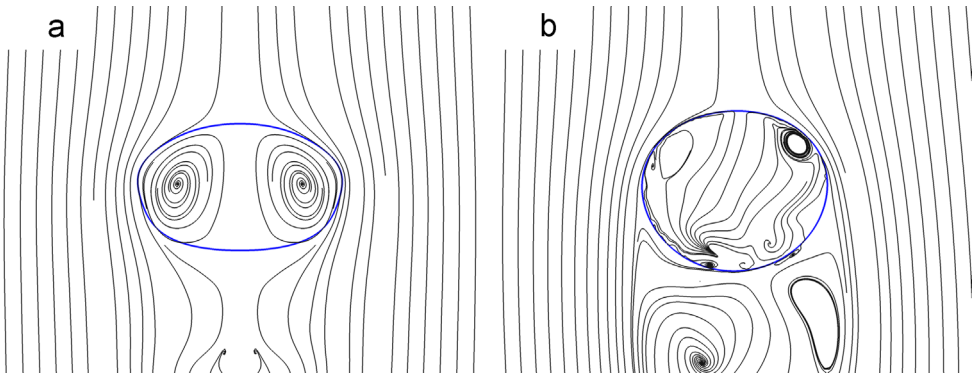

Fig. 10. Streamlines obtained from a simulation without (a) and with (b) Marangoni convection.

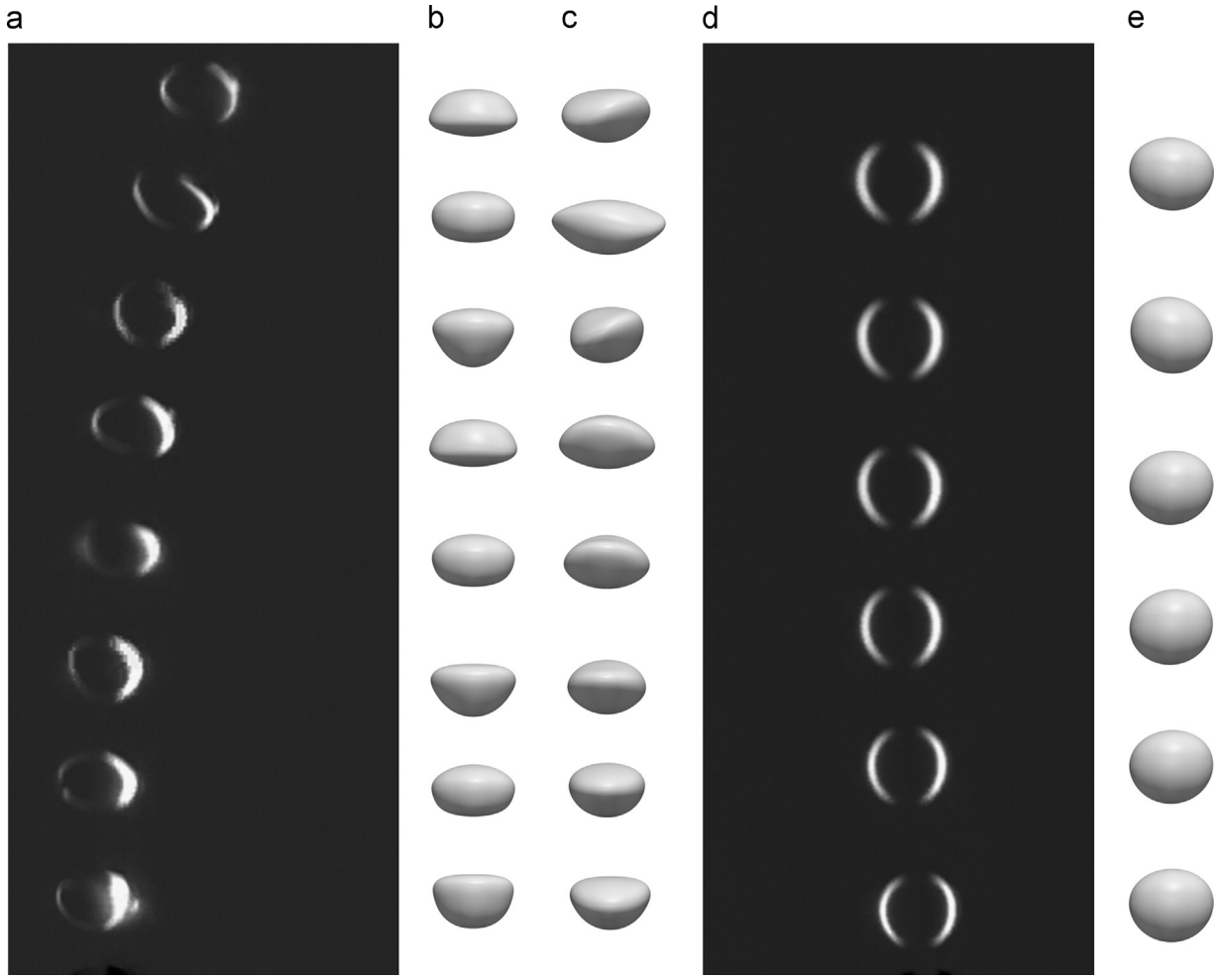

Fig. 11. Droplet shapes: (a) experimental results without Marangoni convection, (b) simulation results for droplet initialised as a sphere, (c) simulation results for droplet initialised as a rotated ellipsoid, (d) experimental results with Marangoni convection ($c_{A0} = 30$ g/L), and (e) simulation results with Marangoni convection ($c_{A0} = 30$ g/L).

For the experimental investigation, every endeavour has been made to avoid impurities which would change the fluid dynamic behaviour of the droplet. The droplet was filmed with high-speed cameras, and transient rise velocities, droplet shapes and trajectories were obtained. To study the droplets with CFD simulations, a code based on the level set method was implemented in the open-source CFD-toolbox OpenFOAM®. Full three-dimensional simulations with and without Marangoni convection were carried out.

The fluid dynamic behaviour of a droplet without Marangoni convection can be considered as a reference case to quantify Marangoni effects. Regarding the characteristic rise velocity of a droplet without Marangoni effects, a good agreement of experimental and numerical results was achieved. However, for a droplet initialised as a sphere, significant deviations from the experimental data with respect to the frequency and the amplitude of the velocity oscillations were found. It was shown that the initial droplet shape influences the simulated rise behaviour, and a better agreement was found for a droplet initialised as a rotated ellipsoid. It should be noted that an ellipsoid is closer to the initial conditions in the experiments, where a retracting capillary was used to form and detach the droplets, causing an initial deformation. Simulated and experimental droplet shapes were in

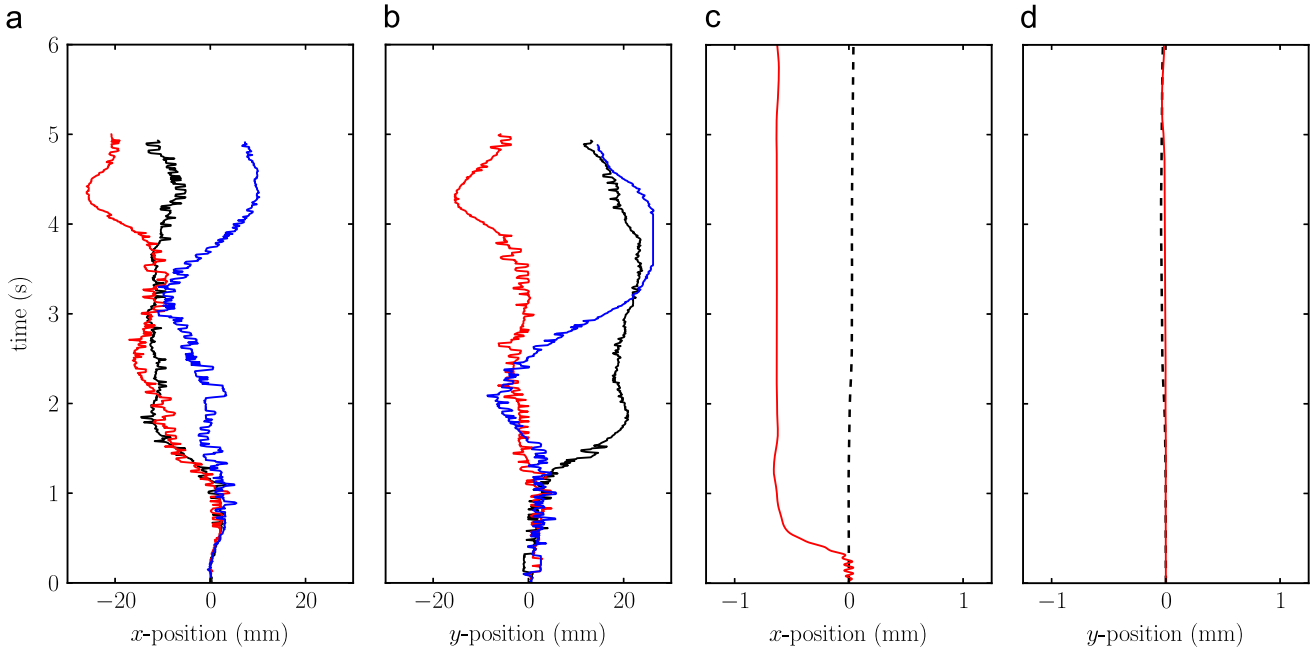

Fig. 12. Droplet trajectories without Marangoni convection ($c_{A0} = 0$ g/L): Three experimental sequences ((a) and (b)), simulation results for a droplet initialised as a sphere (dashed line) and as a rotated ellipsoid (continuous line) ((c) and (d)).

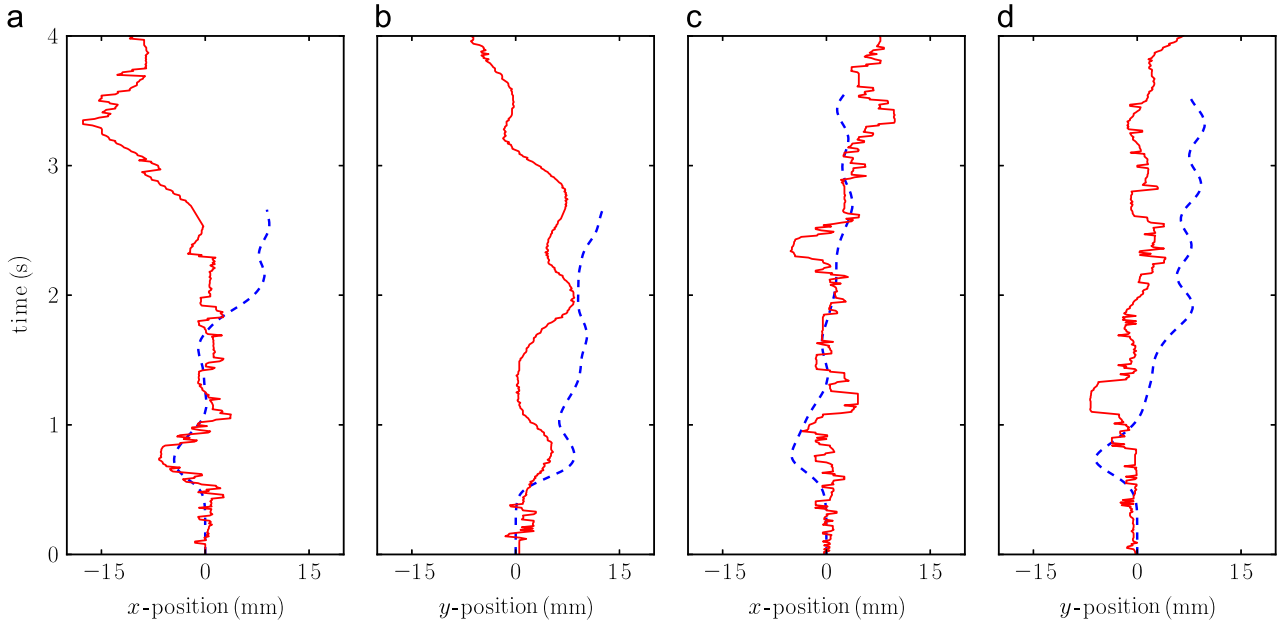

Fig. 13. Droplet trajectories with Marangoni convection: Simulation results (dashed line) and experimental data (continuous line) for initial concentrations of $c_{A0} = 7.5$ g/L ((a) and (b)) and $c_{A0} = 30$ g/L ((c) and (d)).

reasonable agreement, even though the experimental droplet shapes showed stronger asymmetries. These asymmetries led to deviations from the vertical rise path in the experiments, while the simulated droplets rose in an essentially straight path.

It was shown that Marangoni convection reduces the rise velocity, in accordance with the observations for smaller circulating droplets in previous studies. Furthermore, the results reveal that this effect depends on the initial concentration of acetone. Even though the experimental rise velocities showed stronger oscillations, the experimental and the simulated data for the characteristic rise velocity were in very good agreement. Due to the reduced rise velocity, the droplets deform less significantly, a trend which was confirmed both experimentally and numerically. A good agreement was found for the transient droplet trajectories. Despite the fact that the droplets show only slight asymmetries, path oscillations were observed. Consequently, the results suggest that the irregular flow patterns induced by Marangoni effects lead to the path oscillations.

In our opinion, differences between simulations and experiments with Marangoni convection stem mainly from an insufficient grid resolution of the mass transfer. In this respect, sub-grid models for mass transfer might help to achieve better results in the future (cf. Aboulhasanzadeh et al., 2012; Bothe and Fleckenstein, 2013). Nevertheless, the general trend observed in the experiments is well reproduced in the simulations, and we expect to gain further valuable insights in the complex transport phenomena at moving boundaries with CFD simulations in the future.

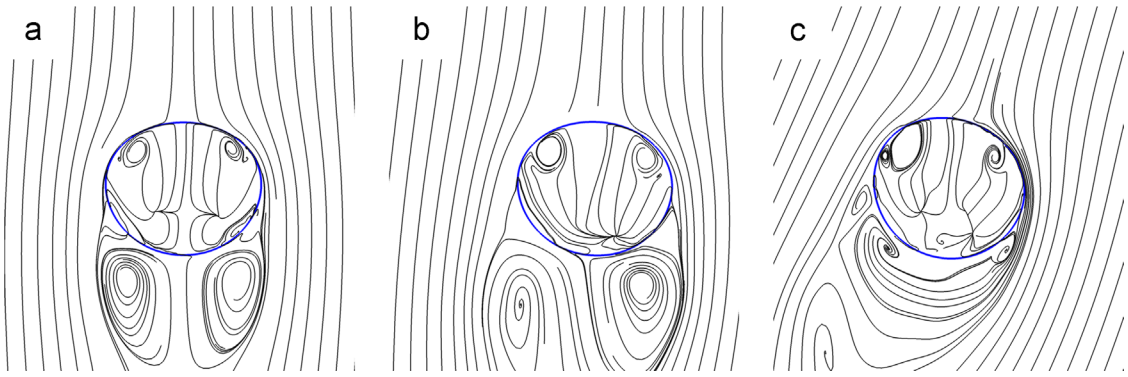

Fig. 14. Streamlines obtained from a simulation with Marangoni convection ($c_{A0} = 30$ g/L) at times 0.3 s, 0.45 s and 0.6 s (from left to right).

Acknowledgments

Simulations were performed at the Paderborn Center for Parallel Computing PC^2. We would like to thank the staff of PC^2 and in particular Mr. Axel Keller for their support.

References

Aboulhasanzadeh, B., Thomas, S., Taeibi-Rahni, M., Tryggvason, G., 2012. Multiscale computations of mass transfer from buoyant bubbles. Chem. Eng. Sci. 75, 456–467.

Bäumler, K., Wegener, M., Paschedag, A.R., Bänsch, E., 2011. Drop rise velocities and fluid dynamic behavior in standard test systems for liquid/liquid extraction—experimental and numerical investigations. Chem. Eng. Sci. 66 (3), 426–439.

Bertakis, E., Groß, S., Grande, J., Fortmeier, O., Reusken, A., Pfennig, A., 2010. Validated simulation of droplet sedimentation with finite-element and level-set methods. Chem. Eng. Sci. 65 (6), 2037–2051.

Bothe, D., Fleckenstein, S., 2013. A volume-of-fluid-based method for mass transfer processes at fluid particles. Chem. Eng. Sci. 101, 283–302.

Brackbill, J.U., Kothe, D.B., Zemach, C., 1992. A continuum method for modeling surface tension. J. Comput. Phys. 100 (2), 335–354.

Burghoff, S., Kenig, E.Y., 2006. A CFD model for mass transfer and interfacial phenomena on single droplets. AIChE J. 52 (12), 4071–4078.

Dijkhuizen, W., Van Sint Annaland, M., Kuipers, H., 2005. Numerical investigation of closures for interface forces in dispersed flows using a 3D front tracking model. In: Proceedings of 4th International Conference on CFD in the Oil and Gas, Metallurgical & Process Industries. SINTEF/NTNU, 6–8 June 2005, Trondheim, Norway.

Eiswirth, R.T., Bart, H.J., Atmakidis, T., Kenig, E.Y., 2011. Experimental and numerical investigation of a free rising droplet. Chem. Eng. Process. 50 (7), 718–727.

Eiswirth, R.T., Bart, H.J., Atmakidis, T., Kenig, E.Y., 2013. Experimentelle und numerische Untersuchung des Tropfenaufstiegs. Chem. Ing. Techn. 85 (6), 944–954.

Engberg, R.F., Wegener, M., Kenig, E.Y., 2014a. Numerische Simulation der konzentrationsinduzierten Marangonikonvektion an Einzeltropfen mit verformbarer Phasengrenze. Chem. Ing. Tech. 86 (1-2), 185–195.

Engberg, R.F., Wegener, M., Kenig, E.Y., 2014b. The impact of Marangoni convection on fluid dynamics and mass transfer at deformable single rising droplets — A numerical study. Chem. Eng. Sci. 116, 208–222, http://dx.doi.org/10.1016/j.ces.2014.04.023.

Engberg, R.F., Kenig, E.Y., 2014. Numerical simulation of rising droplets in liquid-liquid systems: A comparison of continuous and sharp interfacial force models. Int. J. Heat Fluid Flow, http://dx.doi.org/10.1016/j.ijheatfluidflow.2014.05.003.

Francois, M.M., Cummins, S.J., Dendy, E.D., Kothe, D.B., Sicilian, J.M., Williams, M.W., 2006. A balanced-force algorithm for continuous and sharp interfacial surface tension models within a volume tracking framework. J. Comput. Phys. 213 (1), 141–173.

Gross, S., 2008. Numerical Methods for Three-dimensional Incompressible Two-phase Flow Problems (Ph.D. thesis). RWTH Aachen, Germany.

Haroun, Y., 2008. Etude du transfert de masse réactif Gaz-Liquide le long de plans corrugués par simulation numérique avec suivi d'interface (Ph.D. thesis). Université de Toulouse, France.

Haroun, Y., Legendre, D., Raynal, L., 2010a. Direct numerical simulation of reactive absorption in gas–liquid flow on structured packing using interface capturing method. Chem. Eng. Sci. 65 (1), 351–356.

Haroun, Y., Legendre, D., Raynal, L., 2010b. Volume of fluid method for interfacial reactive mass transfer: application to stable liquid film. Chem. Eng. Sci. 65 (10), 2896–2909.

Hartmann, D., Meinke, M., Schroder, W., 2010. The constrained reinitialization equation for level set methods. J. Comput. Phys. 229 (5), 1514–1535.

Hayashi, K., Tomiyama, A., 2012. Effects of surfactant on terminal velocity of a Taylor bubble in a vertical pipe. Int. J. Multiphase Flow 39, 78–87.

Henschke, M., Pfennig, A., 1999. Mass-transfer enhancement in single-drop extraction experiments. AIChE J. 45 (10), 2079–2086.

Issa, R.I., 1986. Solution of the implicitly discretized fluid flow equations by operator-splitting. J. Comput. Phys. 62 (1), 40–65.

Jasak, H., Weller, H.G., Gosman, A.D., 1999. High resolution NVD differencing scheme for arbitrarily unstructured meshes. Int. J. Numer. Meth. Fluids 31 (2), 431–449.

Jiang, G.S., Peng, D., 2000. Weighted ENO schemes for Hamilton–Jacobi equations. SIAM J. Sci. Comput. 21 (6), 2126–2143.

Kang, M., Fedkiw, R.P., Liu, X.-D., 2000. A boundary condition caption method for multiphase incompressible flow. J. Sci. Comput. 15 (3), 323–360.

Kothe, D.B., 1998. Perspective on Eulerian finite-volume methods for incompressible interfacial flows. In: Kuhlmann, H.C., Rath, H. (Eds.), Free Surface Flows, CISM Courses and Lectures 391. Springer, Berlin, pp. 267–331.

Krishna, P.M., Venkateswarlu, D., Narasimhamurty, G.S.R., 1959. Fall of liquid drops in water. Terminal velocities. J. Chem. Eng. Data 4 (4), 336–340.

Liu, X.D., Fedkiw, R.P., Kang, M.J., 2000. A boundary condition capturing method for Poisson's equation on irregular domains. J. Comput. Phys. 160 (1), 151–178.

Misek, T., Berger, R., Schroter, J., 1985. Standard test systems for liquid extraction. Institute of Chemical Engineering, EFCE Publication Series 46.

Osher, S., Sethian, J., 1988. Fronts propagating with curvature-dependent speed: algorithms based on Hamilton–Jacobi formulations. J. Comput. Phys. 79 (1), 12–49.

Rusche, H., 2002. Computational Fluid Dynamics of Dispersed Two-Phase Flows at High Phase Fractions (Ph.D. thesis). Imperial College of Science, Technology & Medicine, London.

Steiner, L., Oezdemir, G., Hartland, S., 1990. Single-drop mass transfer in the water-toluene-acetone system. Ind. Eng. Chem. Res. 29 (7), 1313–1318.

Sussman, M., Smereka, P., Osher, S., 1994. A level set approach for computing solutions to incompressible two-phase flow. J. Comput. Phys. 114 (1), 146–159.

Tomiyama, A., Celata, G.P., Hosokawa, S., Yoshida, S., 2002. Terminal velocity of single bubbles in surface tension force dominant regime. Int. J. Multiph. Flow 28 (9), 1497–1519.

Wang, J.F., Wang, Z.H., Lu, P., Yang, C., Mao, Z.S., 2011. Numerical simulation of the Marangoni effect on transient mass transfer from single moving deformable drops. AIChE J. 57 (10), 2670–2683.

Wang, Z.H., Lu, P., Wang, J.F., Yang, C., Mao, Z.S., 2013. Experimental investigation and numerical simulation of Marangoni effect induced by mass transfer during drop formation. AIChE J. 59 (11), 4424–4439.

Wegener, M., Grünig, J., Stüber, J., Paschedag, A.R., Kraume, M., 2007. Transient rise velocity and mass transfer of a single drop with interfacial instabilities—experimental investigations. Chem. Eng. Sci. 62 (11), 2967–2978.

Wegener, M., Paschedag, A.R., Kraume, M., 2009a. Mass transfer enhancement through Marangoni instabilities during single drop formation. Int. J. Heat Mass Transf. 52 (11–12), 2673–2677.

Wegener, M., Fèvre, M., Paschedag, A.R., Kraume, M., 2009b. Impact of Marangoni instabilities on the fluid dynamic behaviour of organic droplets. Int. J. Heat Mass Transf. 52 (11–12), 2543–2551.

Wegener, M., Eppinger, T., Bäumler, K., Kraume, M., Paschedag, A.R., Bänsch, E., 2009c. Transient rise velocity and mass transfer of a single drop with interfacial instabilities—numerical investigations. Chem. Eng. Sci. 64 (23), 4835–4845.

Wegener, M., Kraume, M., Paschedag, A.R., 2010. Terminal and transient drop rise velocity of single toluene droplets in water. AIChE J. 56 (1), 2–10.

Wegener, M., Paschedag, A.R., 2011. Mass transfer enhancement at deformable droplets due to Marangoni convection. Int. J. Multiphase Flow 37 (1), 76–83.

Winnikow, S., Chao, B.T., 1966. Droplet motion in purified systems. Phys. Fluids 9 (1), 50–61.

Wu, M.M., Gharib, M., 2002. Experimental studies on the shape and path of small air bubbles rising in clean water. Phys. Fluids 14 (7), L49–L52.